Samarium oxide nanoparticle-modified gold electrodes for enhanced Voltammetric sensing of hydrazine and p-Nitrophenol

Wyantuti, Santhy; Ferdiana, Nur Azizah; Zahra, Sahlaa Alifah; Fauzia, Retna Putri; Irkham; Sumeru, Husain Akbar; Jia, Qi; Kurnia, Dikdik; Bahti, Husein H.

DOI
10.1016/j.sbsr.2025.100745

Publication date
2025

Document Version
Final published version

Published in
Sensing and Bio-Sensing Research

Sensing and Bio-Sensing Research 47 (2025) 100745

Contents lists available at ScienceDirect

Sensing and Bio-Sensing Research

journal homepage: www.elsevier.com/locate/sbsr

Samarium oxide nanoparticle-modified gold electrodes for enhanced Voltammetric sensing of hydrazine and p-Nitrophenol

Santhy Wyantuti [a,*], Nur Azizah Ferdiana [a], Sahlaa Alifah Zahra [a], Retna Putri Fauzia [a,b], Irkham [a], Husain Akbar Sumeru [a], Qi Jia [c], Dikdik Kurnia [a], Husein H. Bahti [a,b]

[a] Department of Chemistry, Faculty of Mathematics and Natural Sciences, Universitas Padjadjaran, Jl. Raya Bandung-Sumedang Km. 21 Jatinangor, Sumedang, Jawa Barat 45363, Indonesia
[b] Central Laboratory, Universitas Padjadjaran, Jl. Raya Bandung-Sumedang Km. 21 Jatinangor, Sumedang 45363, Indonesia
[c] Department of Biotechnology, Faculty of Applied Sciences, Delft University of Technology, Van der Maasweg 9, 2629, HZ, Delft, the Netherlands

ARTICLE INFO

Keywords:
Cyclic voltammetry
Electrochemical nanosensor
Hydrazine
Sm_2O_3 nanoparticles
P-Nitrophenol

ABSTRACT

Samarium oxide (Sm_2O_3), such as electrochemical sensors, is a promising material in various application prospects and industries. Additionally, Sm_2O_3 leverages electron transport capabilities, high electrical conductivity, and thermal stability to develop an effective material in electrode modification for detecting hazardous pollutants. Hydrazine and p-nitrophenol are compounds commonly used in producing insecticides, pesticides, pharmaceuticals, and the chemical industry. However, these compounds can become hazardous environmental pollutants and pose serious health risks to humans. Therefore, this research aims to examine the impact of modifying gold electrode (GE) with Sm_2O_3 nanoparticles, characterizing the electrochemical results, and assessing sensor performance through the use of the GE/Sm_2O_3 NP electrode. In this context, the purpose is to detect hydrazine and p-nitrophenol through voltammetry, with analytical parameters including recovery, repeatability, detection limit, quantification limit, and linear range. The results show that the synthesis of Sm_2O_3 nanoparticles and the performance of the sensor and analytical parameters of GE/Sm_2O_3 NP are carried out in detecting hydrazine and p-nitrophenol using the Cyclic Voltammetry (CV) method. Furthermore, the significant increase in the current response validates the improvement of GE conductivity as an electron transporter. The sensor performance has been studied, and analytical parameters have been determined. For hydrazine and p-nitrophenol, the values are recovery of 98.74 % and 99.01 %, repeatability of 99.42 % and 98.45 %, limit of detection (LoD) of 0.4684 μM and 0.50332 μM, limit of quantification (LoQ) of 1.4194 μM and 1.5252 μM, and linear concentration range for both analytes from 0.1 μM to 7 μM.

1. Introduction

Samarium oxide (Sm_2O_3) is a rare earth metal oxide which has been extensively studied in various branches of materials science due to its unique properties and potential applications [1,2]. Sm_2O_3 in nano size holds promising prospects with potential applications in different fields including solar cells, nanoelectronics, semiconductor gases, electrochemical sensors, and as highly active catalysts in some oxidation reactions [3,4]. Meanwhile, the development of electrochemical sensors using nanotechnology has become an intriguing candidate for analysis with increased sensitivity and stability [5–12]. This nanotechnology material offers several advantages, such as rapid response, good portability, easy operation, excellent selectivity, efficiency, low cost, higher accuracy, low detection limits, and the use of fewer reagents compared to chromatogram-based techniques [13,14]. Rare earth metal oxide nanoparticles, particularly Sm_2O_3, exhibit excellent electrical properties, increasing the suitability of developing new electrochemical sensors with improved sensitivity and selectivity toward target molecules [4,15]. The properties of nanomaterials are influenced by their size and architecture, specifically the surface properties [16]. Higher surface/volume ratio in nanomaterials offers advantages such as rapid reaction kinetics and, resultantly, the materials become excellent candidates for analytical detection [17].

In the synthesis process of Sm_2O_3, polyethylene glycol (PEG) can be used as a template to form and determine the size of particle structure pores, resulting in smaller, uniformly shaped, easily soluble, and

* Corresponding author.
E-mail address: santhy.wyantuti@unpad.ac.id (S. Wyantuti).

https://doi.org/10.1016/j.sbsr.2025.100745
Received 4 November 2024; Received in revised form 15 January 2025; Accepted 20 January 2025
Available online 21 January 2025

biocompatible spherical nanoparticles [18,19]. The particle size of nanoparticles will be reduced, and the distribution size will be homogenized due to the role of PEG in preventing agglomeration [18,20,21]. It has been reported that PEG positively increases the crystal nucleation rate and nanoparticle aggregation [22,23]. The properties of nanoparticles will determine the sensor resistance and thus shall be controlled [6]. These Sm_2O_3 nanoparticles can leverage electron transport capabilities, high electrical conductivity, and thermal stability to develop an effective material in electrochemical sensors [24,25].

Hydrazine and nitroaromatic compounds are frequently used in the chemical industry to produce insecticides, pesticides, and pharmaceuticals. However, these compounds are highly stable nature and low degradation efficiency pose serious health risks to humans. Hydrazine is carcinogenic and harmful to aquatic ecosystems, while p-nitrophenol is toxic to plants, animals, and humans, causing respiratory, liver, and nervous system damage. Detecting these compounds is crucial to prevent environmental contamination, protect human health, and ensure effective industrial waste management [26,27]. The concentration of these compounds in both industries, namely waste and environment, should be controlled and monitored regularly.

Several analytical instrument methods can be used to detect hydrazine and p-nitrophenol, including colorimetry, X-rays, fluorescence emission spectroscopy, inductively coupled plasma spectroscopy, atomic absorption spectroscopy, mass spectroscopy, and chromatography [26,28]. These methods efficiently detect both pollutants but include complex functions, high processing costs, and require professional expertise for data analysis [29–31].

Several research projects have been conducted to measure a particular compound using an electrochemical sensor [32,33]. Nanoparticles of diverse metal and metal oxide have been studied for sensing hydrazine using the electroanalytical method [34,35]. Metal nanoparticles, either as electrodes or electrode modifications, have been explored to overcome the slow detection of hydrazine and high overpotentials [36,37]. Nanoparticle gold is the most explored electrode for electrochemical sensors, though it is expensive [34,37]. Other metals, such as Zinc [36,38], Copper [39,40], and Silver [41] have also been explored, with promising results.

Sm_2O_3 (samarium(III) oxide) stands out among other metals and metal oxides for its unique properties that enhance its importance in electrochemical applications. One of its key advantages is its superior catalytic activity, enabled by the multiple oxidation states of samarium (Sm^{3+} and Sm^{2+}), which facilitate efficient electron transfer during redox reactions [42]. This makes Sm_2O_3 highly effective for detecting compounds like hydrazine and p-nitrophenol at lower energy barriers compared to materials like ZnO or TiO_2 [43,44]. Additionally, Sm_2O_3 has a strong affinity for functional groups such as amino ($-NH_2$) and hydroxyl (-OH) groups, enabling selective interactions with target analytes and reducing interference from other compounds in complex samples [42]. This level of selectivity is often unmatched by other materials.

Another critical advantage is its exceptional chemical stability and resistance to corrosion, making it durable in harsh environments, such as highly acidic or basic conditions, where other oxides like Fe_2O_3 or ZnO might degrade [45,46] This durability ensures the long-term usability of Sm_2O_3-modified electrodes in challenging applications, such as industrial effluent monitoring or polluted water analysis. The unique 4f electron configuration of samarium also plays a significant role in enhancing its catalytic and electronic properties, giving it an edge over transition metal oxides that lack this feature. Lastly, Sm_2O_3 provides a cost-effective alternative to noble metals like platinum or palladium. While delivering comparable performance, its relative affordability and sustainability make it an attractive choice for developing advanced electrochemical sensors, particularly for environmental and industrial monitoring [42,47,48].

The preliminary research determined the optimal conditions for synthesizing Sm_2O_3 nanoparticles with PEG as a template using the hydrothermal method based on the Box-Behnken experimental design. The parameters influencing the synthesis process are mass of Sm_2O_3, reaction temperature, and time at low, medium, and high levels. Furthermore, the hydrothermal process holds promising prospects and advantages due to the economic nature, flexible reaction constraints, and prospective ability for large-scale particle production [19,49]. Based on the background, Sm_2O_3 nanoparticles are applied under optimal hydrothermal conditions using the Box-Behnken experimental design to modify gold electrode (GE) as an electrochemical sensor for the detection of hydrazine and p-nitrophenol through voltammetry. The Sm_2O_3 nanoparticles-modified GE electrode is a promising candidate to be applied for enhancing voltammetric sensing of hydrazine and p-nitrophenol.

2. Experimental

2.1. Materials

The materials used include demineralized water, 65 % nitric acid (HNO_3, p.a Merck, Indonesia), acetone, butyl carbitol acetate (BCA) (Merck, Indonesia), sodium hydroxide (NaOH, p.a Merck, Indonesia), hydrazine (p.a Merck, Indonesia), phosphate buffer saline (PBS) pH 7.4 (p.a Merck, Indonesia), p-nitrophenol (p.a Merck, Indonesia), polyethylene glycol 6000 (PEG-6000, p.a Sigma Aldrich, Indonesia), and samarium oxide (Sm_2O_3, 99,9 %) (p.a Sigma Aldrich, Indonesia).

2.2. Equipment

The equipment used comprises common glassware typically found in the Chemistry Department Research Laboratory. Additionally, other supporting equipment includes hydrothermal autoclave, gold working electrode (GE) (GSI Technologies, USA), dry-type Ag/AgCl reference electrode eDAQ, platinum wire counter electrode, Field Emission Scanning Electron Microscope (FESEM) (Inspect F50 by FEI, USA), Field Emission Transmission Electron Microscope – Energy Dispersive X-Ray spectroscopy (FETE-EDX) (Tecnai G2 by FEI, USA), hot plate (IKA C-MAG HS 7), magnetic stirrer (Eppendorf), analytical balance (Mettler Toledo AL204), Metrohm® μAutolab potentiostat connected to a computer using Nova 2.1 software, Tabletop Microscope (Hitachi SU3 500), micropipette (Eppendorf), microtubes, micropipette tips, and X-Ray Diffraction (D8 Advance by Bruker, USA).

2.3. Procedure

2.3.1. Preparation of pH 7.4 phosphate buffer saline (PBS) solution

A pH 7.4 PBS solution was prepared by dissolving 1 PBS tablet in 100 mL demineralized water and stirring until homogeneous. Furthermore, the pH was adjusted by adding 0.1 M NaOH or HCl until reaching a pH of 7.4.

2.3.2. Synthesis of samarium oxide (Sm_2O_3) nanoparticles

i. *Preparation of 0.9 mmol Sm_2O_3 0,9 Solution*

Solid Sm_2O_3 weighing 0.3138 g was placed in a 50 mL beaker glass. Subsequently, 20 mL demineralized water was added, stirred with a magnetic stirrer, and heated on a hot plate, resulting in a 0.9 mmol Sm_2O_3 0.9 mmol.

ii. *Melting of Polyethyeleneglycol-6000 (PEG-6000) Solid*

PEG-6000, weighing 10 g, was placed in a 50 mL beaker glass and heated on a hot plate for 20 min until the solid melted.

iii. *Mixing Sm_2O_3 Solution with PEG-6000*

Polyethylene glycol 6000 (PEG-6000) and samarium oxide (Sm_2O_3)

solution as precursors were grown in situ. A 0.9 mmol solution of Sm_2O_3 was added to the 10-g PEG-6000 which had been melted drop by drop, stirred with a magnetic stirrer, and heated with a hot plate until both mixtures dissolved completely before cooling at room temperature.

iv. *Synthesis of Sm_2O_3-coated PEG-6000 Nanoparticles by Autoclave (Hydrothermal Method)*

A mixture of Sm_2O_3 solution with PEG-6000 was transferred into the autoclave Teflon at room temperature. The autoclave was put in the oven to be heated at 180 °C and the synthesis time was 5 h until colloids formed. The colloids in the heat-treated autoclave were cooled to room temperature.

v. *Filtration of Sm_2O_3 Deposits from Autoclave Synthesis*

The mixture of Sm_2O_3 solution with PEG-6000 synthesized via autoclave was filtered using a Buchner funnel and a vacuum device. Before screening, the filter paper used was weighed first and recorded in mass. The resulting precipitate was washed several times using acetone and ethanol to remove excess polymer.

vi. *Filtration of Sm_2O_3 Deposits from Autoclave Synthesis*

The precipitate obtained from filtering with the Buchner funnel was put into the oven for the drying process at 60 °C for 24 h. Subsequently, Sm_2O_3 powder was obtained and crushed using a grinder and mortar. The resulting powder was weighed and the yield mass obtained, the latter of which was then characterized using an Scanning Electron Microscope (SEM).

2.3.3. Gold electrode (GE) modification with Sm_2O_3 nanoparticles

The synthesized Sm_2O_3 nanoparticles were used for GE modification for hydrazine and p-nitrophenol detection. The first preparation with a surface area of 2.85 mm^2 was cleaned using alumina slurry and washed with demineralized water via sonication. After the electrode was dried at room temperature, the GE surface was coated with Sm_2O_3 nanoparticles using butyl carbitol acetate (BCA) as a binder. This drop-cast electrode was dried at 60–65 °C for 3 h until a homogeneous and dry nanoparticle layer was formed on the surface for electrochemical characterization.

2.3.4. GE/Sm_2O_3 modified application test with cyclic voltammetry (CV)

In electrochemical measurements with cyclic voltammetry (CV), a cell with three electrodes was used. Modified GE with Sm_2O_3 nanoparticles was employed as the working electrode, Ag/AgCl in KCl 1 M as the reference/comparison electrode, and the Pt electrode as the counter/auxiliary electrode.

GE before and after the modification was tested for electrochemical properties in 0.1 M PBS (pH 7) with each analyte concentration (hydrazine and p-nitrophenol) at 2 Mm. This showed a potential range of −1 to 1 V and − 1 to 2 V for hydrazine and p-nitrophenol vs Ag/AgCl and a scan rate of 0.06 V/s.

2.3.5. Scan rate variation in electrochemical properties analysis of GE/Sm_2O_3 modified results for hydrazine and p-Nitrophenol detection

Scan rate variations were performed to investigate the electron transfer mechanism for GE-modified Sm_2O_3 nanoparticles in the presence of hydrazine analyte and p-nitrophenol. Measurements were made at different variations of 60–900 mV/s with analyte solutions (hydrazine and p-nitrophenol), each at a concentration of 2 μM in PBS 0.1 M, pH 7.

2.3.6. Determination of linear calibration curve at GE/Sm_2O_3 electrode for hydrazine and p-Nitrophenol detection

The determination of the linear calibration curve at the GE/Sm_2O_3 electrode was performed by varying the concentration of analytes (hydrazine and p-nitrophenol) at 0.1, 0.3, 0.5, 0.7, 0.9, 1.2, 1.5, and 1.7 μM in 0.1 M PBS solution, pH 7 with a potential range of −1 to 1 V and − 1 to 2 V for hydrazine and p-nitrophenol to Ag/AgCl and a scan rate of 0.06 V/s.

2.3.7. Analytical parameter determination of GE/Sm_2O_3 electrode sensor for hydrazine and p-Nitrophenol detection

The determination of the detection limit of GE/Sm_2O_3 was performed by measuring the concentration providing a linear current, where the measurement was carried out thrice. The regression plot of the current response value versus the concentration of the two analytes determined the regression equation and calculated the linear range of measurement concentration, recovery, repeatability, limit of detection (LoD), and limit of quantification (LoQ). The sensitivity of the developed sensor was determined based on the slope of linear regression for hydrazine and p-nitrophenol.

2.3.8. GE/Sm_2O_3 electrode reproducibility determination for hydrazine and p-Nitrophenol detection

Determination of GE/Sm_2O_3 electrode reproducibility was performed in hydrazine and p-nitrophenol solutions at 1 μM 6 times in the potential range of −1 to 1 V and − 1 to 2 V for hydrazine and p-nitrophenol, with a scan rate of 0.06 V/s.

3. Results and discussion

3.1. Synthesis and characterization of samarium oxide (Sm_2O_3) nanoparticles

3.1.1. Synthesis of samarium oxide (Sm_2O_3) nanoparticles using polyethylene Glycol-6000 (PEG-6000) template

The synthesis of Sm_2O_3 nanoparticles was undertaken via the hydrothermal method using an autoclave (Fig. 1). The reactants were heated in a closed container using a water medium, allowing pressure and temperature to increase rapidly. The synthesis process was carried out at optimum conditions based on the optimization of Box Behnken's experimental design.

The use of polyethylene glycol-6000 (PEG-6000) as a template in the synthesis process was intended to maintain the size of Sm_2O_3 nanoparticles formed during the reaction inside the autoclave. PEG plays a role in improving the stability of nanoparticles by binding oxygen atoms from the PEG hydroxyl group to the surface of nanoparticles. The bond formed is a coordination bond, in which the oxygen of the hydroxyl group acts as an electron donor bonding to Sm_2O_3.

PEG acts as a ligand capable of interacting with samarium atoms to form complex compounds. The chemical structure contains oxygen atoms that allow the ligands to bind to Sm^{3+} ions and form a stable complex. This phenomenon occurs because the surface of Sm_2O_3 has a positive charge, and therefore colloidal stabilization occurs due to the van der Waals force between the negatively charged oxygen in the PEG molecular structure and the positively charged group surrounding the surface of Sm_2O_3. The interaction can maintain the stability of Sm_2O_3 nanoparticles during the synthesis process.

The activity of the particles decreases significantly when PEG is adsorbed by the surface of oxide particles, and the growth rate of colloids on certain surfaces becomes limited. Therefore, the addition of PEG to the reaction system changes the kinetics of the growth process associated with rapid nucleation and leads to the formation of nanoparticle aggregation. As such, the spherical nanoparticles were used [19,54].

3.1.2. Characterization of samarium oxide (Sm_2O_3) nanoparticles with scanning Electron microscope (SEM)

The synthesized Sm_2O_3 powder was characterized using Scanning Electron Microscope (SEM) instruments to determine the surface morphology and size of nanoparticles. The results of the characterization of Sm_2O_3 nanoparticles are shown in Figs. 2 and 3.

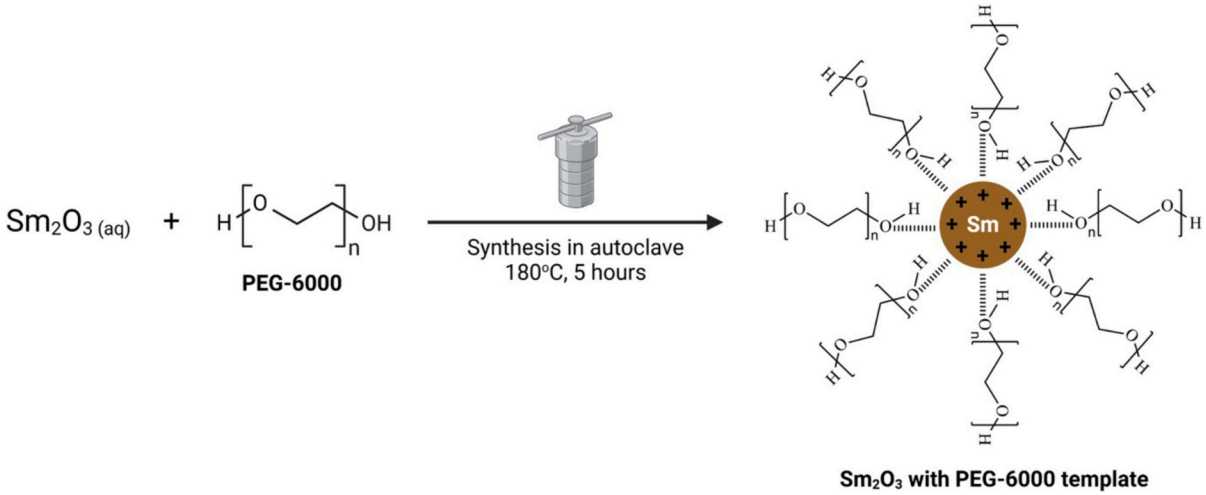

Fig. 1. Schematic illustration of Sm_2O_3 and PEG interaction via hydrothermal synthesis for 5 h at 180 °C.

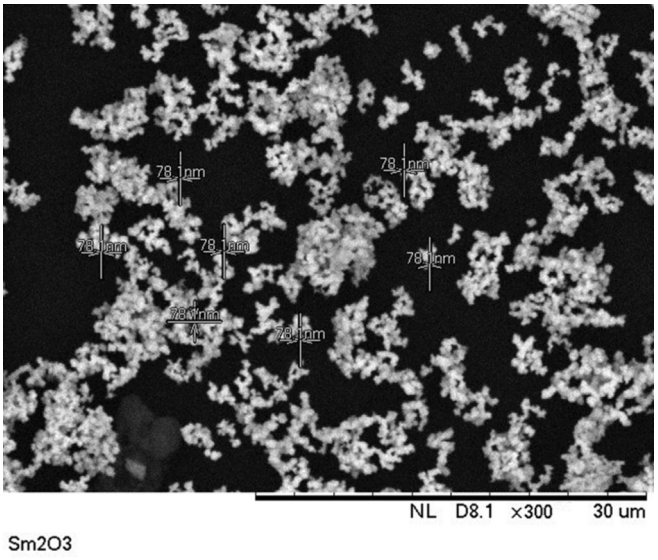

Fig. 2. SEM characterization results of surface morphology and size of Sm_2O_3 nanoparticles at 300× magnification.

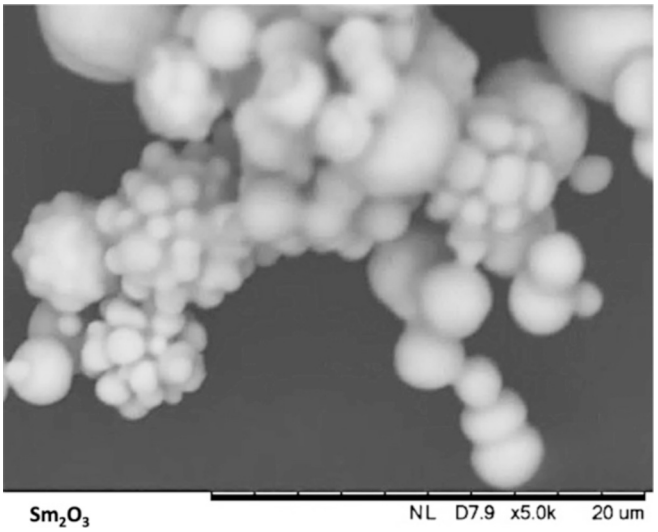

Fig. 3. SEM characterization results of surface morphology of Sm_2O_3 nanoparticles at 5000× magnification.

Based on Figs. 2 and 3, synthesized Sm_2O_3 nanoparticles show spherical shapes. This morphological shape is very important because, when not spherical, the possibility of contact with other nanoparticles will be higher, causing the sample to be more easily aggregated. However, the particles are not evenly distributed, and the resulting shapes vary in small and large sizes.

In addition to the surface morphological analysis of Sm_2O_3 nanoparticles, micrographs of SEM characterization results observed are particle size scales (granules), as shown in Fig. 3. The size of Sm_2O_3 measured from the diameter distance between spherical shapes is 78.1 nm. The particle size is determined using ImageJ software to obtain N amounts. The analysis is performed with a Gaussian method to obtain the particle size value. In determining particle size, the average is also calculated directly using the equation Σ xi/N, where xi is the data point.

Characterization of the SEM in Figs. 2 and 3 was accomplished using a pre-set scale bar. The "Set Scale" information in the ImageJ software was filled with the "Known distance" column for the scale bar indicated in Figs. 1 and 2 as 30 and 20 μm, respectively. The "Unit of length" was used to specify the unit of measurement in SEM images.

3.1.3. Characterization of samarium oxide (Sm_2O_3) nanoparticles with transmission Electron microscope-energy dispersive X-ray spectroscopy (TEM-EDX)

The surface morphology and size of Sm_2O_3 nanoparticles can be characterized using a Transmission Electron Microscope (TEM). The sample preparation process for TEM includes steps to make the sample very thin for the penetration of electrons. Subsequently, the sample was placed on a TEM grid made of copper or carbon. TEM characterization results of Sm_2O_3 nanoparticles are shown in Fig. 4.

In addition, according to the Energy Dispersive X-Ray Spectroscopy (EDX) results in Fig. 5, samarium and oxygen are present in the elemental composition with weight percentages of 65.571 % and 34.429 %, and atomic percentages of 16.851 % and 83.149 %, respectively.

3.1.4. Characterization of samarium oxide (Sm_2O_3)

3.1.4.1. Nanoparticles with X-Ray Diffraction (XRD). An X-Ray Diffraction (XRD) technique was used to investigate the crystal properties of the Sm_2O_3 nanoparticles with Cu Kα (λ = 1.54 Å) radiation at the angles ranging from 10 to 70° for 2θ. XRD characterization is used to determine

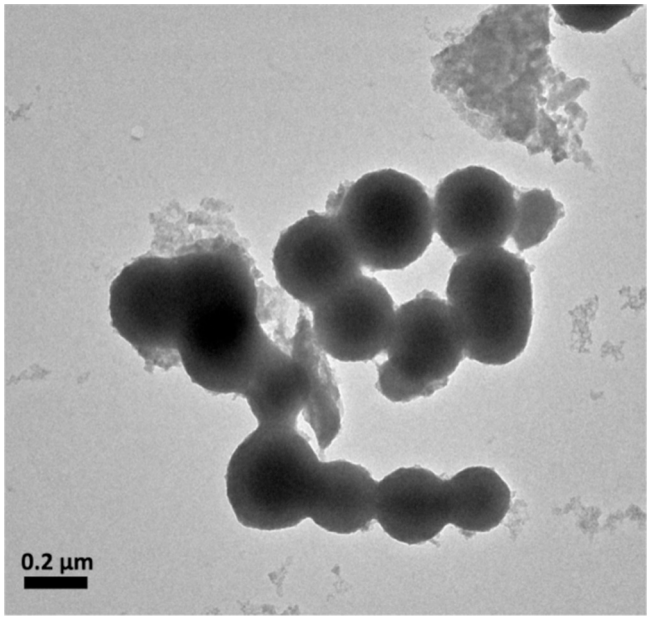

Fig. 4. Characterization results of TEM surface morphology of Sm_2O_3 nanoparticles at 5000× magnification.

the diffraction pattern, size, and crystal structure of Sm_2O_3 nanoparticles synthesized using PEG-6000 as a template. The characterization results are shown in Fig. 6, indicating diffraction peaks corresponding to Sm_2O_3 structure. The XRD pattern is analyzed using X'Pert Highscore Plus software for additional information on the size and crystal properties of the produced nanoparticles.

Based on the diffraction pattern in Fig. 5, Sm_2O_3 nanoparticles' crystal structure is cubic, with peaks at 2θ angles of 23.44°, 28.3°, 32.8°, 47°, and 55.8° (based on JCPDS PDF No. 741807), while the average crystal size is determined to be 45 nm. Additionally, peaks at 19.11° and 23.44° are consistent with PEG diffraction pattern [55].

3.2. Modification of gold electrode (GE) with samarium oxide (Sm_2O_3 NP)

3.2.1. Characterization of the surface of samarium oxide-modified GE (GE/Sm_2O_3 NP) using scanning Electron microscope (SEM)

Gold electrode (GE) modified with Sm_2O_3 nanoparticles (GE/Sm_2O_3 NP was characterized using a Scanning Electron Microscope (SEM) to understand the surface morphology using butyl carbitol acetate (BCA) as a binding agent. Additionally, a comparison was made between bare GE (before modification) and GE/Sm_2O_3 NP, with the characterization results of bare GE and GE/Sm_2O_3 NP shown in Fig. 7.

Based on Fig. 7b, GE modified with Sm_2O_3 nanoparticles shows a denser surface, with molecules covering the electrode surface, compared to the pure GE in Fig. 7a. This shows the successful attachment of GE/Sm_2O_3 to the GE surface for electrochemical characterization in the application as a sensor. The modified electrode surface morphology shows irregular shapes resembling aggregates of Sm_2O_3 nanoparticles with BCA binding agent.

3.2.2. Characterization of GE/Sm_2O_3 performance through electrochemistry using cyclic voltammetry (CV)

Electrochemical characterization was conducted to understand the impact of modifying gold electrode (GE) with Sm_2O_3 nanoparticles as a sensor for the detection of hydrazine and p-nitrophenol. The electrochemical properties focus on the electrocatalysis of hydrazine and p-nitrophenol through Cyclic Voltammetry (CV) analysis. The CV voltammogram results of GE in 0.1 M phosphate buffer saline (PBS) at pH 7.4 are shown in Fig. 8.

Based on Fig. 8, pure GE (bare GE) does not show significant oxidation or reduction signals in PBS pH 7.4 in the potential range of −2.0 V to 1.0 V at a scan rate of 0.06 V/s. A very small oxidation signal is observed at a current of 0.1533 µA. The significant current peaks with an increase in CV analysis conditions for hydrazine detection in PBS solution are shown in Fig. 9.

Fig. 9 shows cyclic voltammograms under different conditions of GE for the detection of 2 µM hydrazine in the potential range of −1.0 V to 1.0 V at a scan rate of 0.06 V/s. In the three conditions represented by different colors, the highest current peaks indicate oxidation signals for hydrazine. In detection with bare GE, shown by the light blue curve, oxidation peak 1 (O1) is visible at a potential of 0.3187 V with a current of 4.1250 µA. Meanwhile, oxidation peak 2 (O2) is at a potential of 0.7226 V with a current of 10.8704 µA.

In Sm_2O_3-modified GE, represented by the dark red curve, there is an

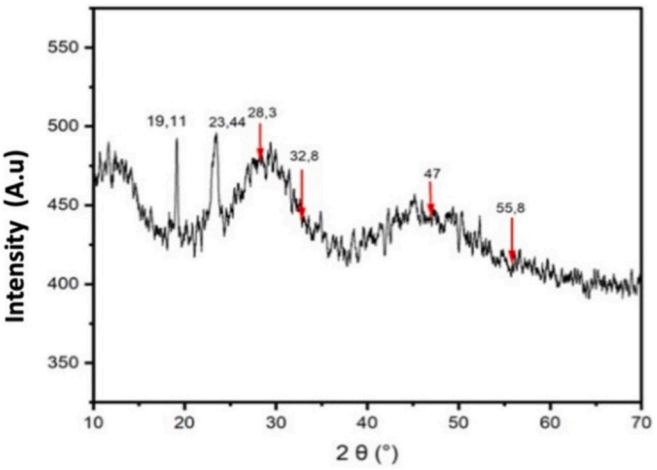

Fig. 6. XRD characterization results of Sm_2O_3 nanoparticles (confirmed on JCPDS PDF No. 741807).

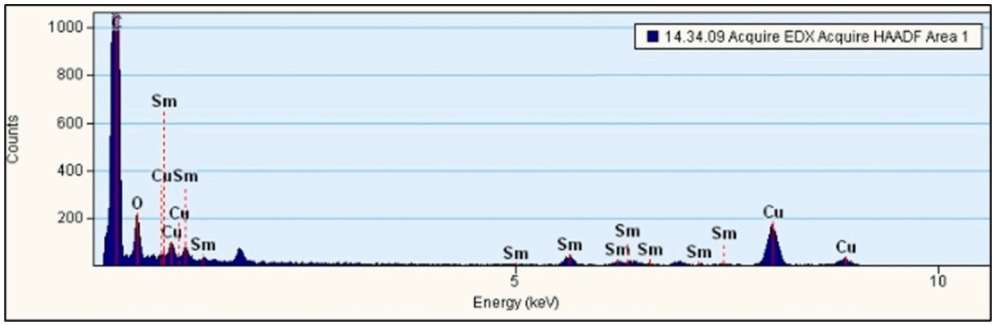

Fig. 5. EDX characterization results of elemental composition in Sm_2O_3 nanoparticles.

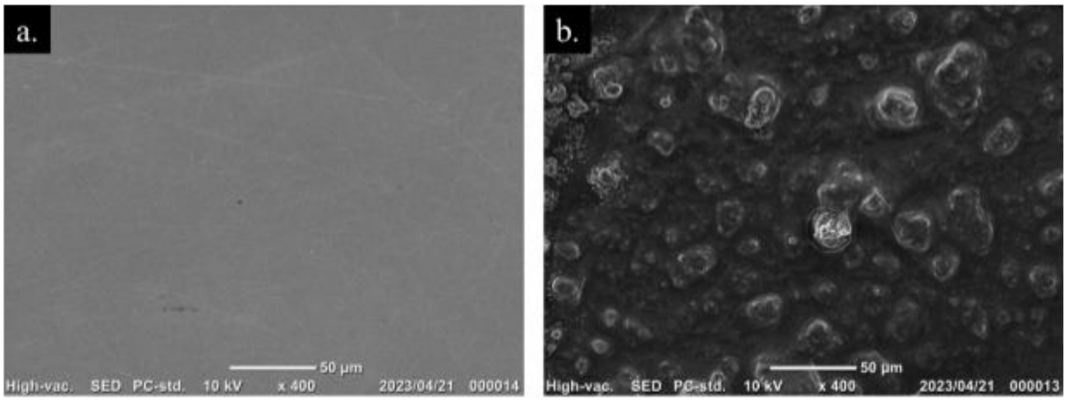

Fig. 7. SEM characterization of the surface of (a) bare GE and (b) GE/Sm_2O_3 NP.

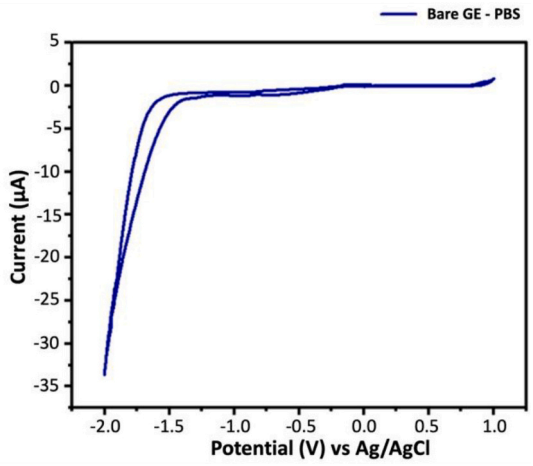

Fig. 8. Cyclic voltammogram for bare GE in 0.1 M PBS (pH 7.4), scan rate 0.06 V/s.

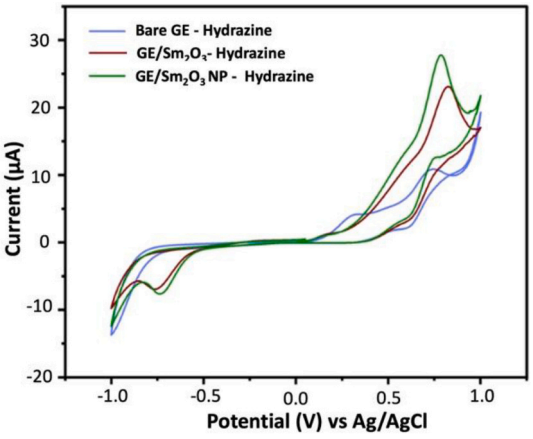

Fig. 9. Comparison of cyclic voltammograms for bare GE, Sm_2O_3-modified GE (GE/Sm_2O_3), and nanoparticle-modified GE (GE/Sm_2O_3 NP) in the detection of 2 µM hydrazine (in 0.1 M PBS (pH 7.4)), scan rate 0.06 V/s.

increase in current at a potential of 0.7821 V with a peak of 23.1018 µA. An increase is observed in nanoparticle-modified GE, shown by the dark green curve, at a potential of 0.78125 V with a current of 28.4973 µA. This shows the highest peak among the three electrode variations with the same analyte concentration. Therefore, the modification of GE with Sm_2O_3 nanoparticles can provide a larger current signal in hydrazine detection.

Based on the study [26] regarding the hydrazine detection using Gd_2O_3-modified GE, a well-defined voltammetric signal is observed at a potential of 0.68 V. Cyclic voltammogram for Sm_2O_3 nanoparticle-modified GE (GE/Sm_2O_3 NP) shows a reduction peak at a potential of −0.7251 V with a current of −1.1407 µA. A similar cyclic voltammogram for hydrazine detection is also shown by [56]. Electrochemical characterization of various GE conditions for the p-nitrophenol analyte in the PBS solution is investigated in Fig. 9.

Based on Fig. 10, cyclic voltammograms under different conditions of GE for the detection of 2 µM p-nitrophenol show a significant increase in current from bare to Sm_2O_3-modified GE. In p-nitrophenol detection with bare GE, indicated by the blue curve, a set of reversible redox peaks occurs with oxidation and current peak at a potential of 1.2597 V and 7.2662 µA, respectively. Meanwhile, the reduction peak occurs at a potential of 0.6494 V with a peak current of −1.6763 µA. There is an increase in the peaks of oxidation and reduction of the Sm_2O_3-modified GE, as indicated in the red-colored curve with reversible redox peaks. The oxidation (O1) and reduction (R1) peaks occur at 1.2212 V and 0.6494 V with a current of 15.6341 µA and − 2.7365 µA, respectively. Other irreversible reduction peaks, namely R2 and R3, occur at a potential of −0.4907 V and 0.6494 V with a current of −2.1420 µA and − 2.3352 µA. Subsequently, the highest peaks of oxidation and reduction occur on GE modified with Sm_2O_3 nanoparticles, as shown by the purple-colored curve with reversible redox peaks. The oxidation and reduction peaks occur at 1.2206 V and 0.6665 V with currents of 35.9863 µA and − 2.8170 µA. Other irreversible reduction peaks, namely R2 and R3, occur at a potential of −0.5493 V and 0.6665 V with

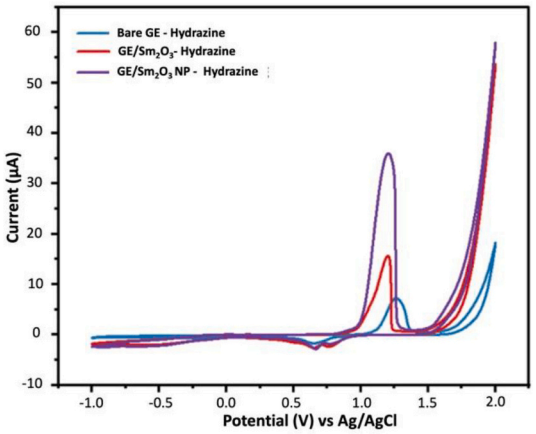

Fig. 10. Comparison of cyclic voltammograms for bare GE, Sm_2O_3-modified GE (GE/Sm_2O_3), and nanoparticle-modified GE (GE/Sm_2O_3 NP) in the detection of 2 µM p-nitrophenol (in 0.1 M PBS (pH 7.4)).

a current of −2.2345 μA and − 2.8170 μA, respectively.

The results reported that p-nitrophenol has shown three electrochemical responses with two subsequent processes, including reduction and redox couple progression. This occurs due to the two-electron reduction-oxidation reaction in 4-aminophenol. Meanwhile, the reduction peak is associated with the formation of a hydroxylamine group from the nitro group in p-nitrophenol.

With Sm_2O_3 nanoparticles as a modifier for GE, a significant increase in peak current for each analyte has been observed. This verifies the utility of the formed nanoparticles for electroanalytical purposes. The increase in peak current is attributed to the enhanced electrode conductivity resulting from the surface functionalization of GE using Sm_2O_3. The formed Sm_2O_3 nanoparticles have the potential to modify electrochemical sensor electrodes as efficient electron transporters for the electrocatalysis of hydrazine and p-nitrophenol.

The active surface area is also found to increase from 11.55 to 14.82 cm^2 after the nanoparticles' modification, which will lead to an enhancing of GE conductivity and serve as an efficient electron transporter for the electrocatalysis of hydrazine and p-nitrophenol.

3.3. Mechanism of measuring hydrazine and p-Nitrophenol by voltammetry

Based on the mechanism in Fig. 10, cyclic voltammetry (CV) response explains that the hydrazine oxidation process includes two electron changes indicating the existence of electrocatalytic activity between gold electrode (GE) modified Sm_2O_3 GE/Sm_2O_3 and hydrazine in the phosphate buffer saline (PBS) solution pH 7.4. Indeed, p-nitrophenol analyte has a nitro and hydroxyl group that can be reduced and oxidized. The irreversible and reversible reactions in the detection of p-nitrophenol include the gain and exchange of four and two electrons. Furthermore, the irreversible reduction process is characterized by the formation of 4-hydroxyaminophenol, and two paired redox peaks indicate the oxidation of 4-hydroxyaminophenol to 4-nitrosophenol. The number of electrons included in the reaction (n) for hydrazine and p-nitrophenol is calculated based on the following Randles-Sevcik Eq. [57]:

$$ip = (2.69\ x\ 10^5) n^{\frac{3}{2}} A D^{\frac{1}{2}} v^{\frac{1}{2}} C \quad (1)$$

where n = equivalent number of electrons exchanged during the redox process,A = active surface area of the working electrode (cm^2).C = bulk hydrazine concentration (mol/cm^3).D = diffusion coefficient (cm^2/s).v = scan rate voltage (*scan rate*) (V).

In addition, based on this equation and various scan rate CV measurement the active surface area was also found to increase from 2.85 to 3.66 mm^2 after the nanoparticles modification which will affect to enhancing GE conductivity and serving as an efficient electron transporter for the electrocatalysis of hydrazine and p-nitrophenol.

3.4. Analysis of scan rate variations in Voltammetric measurements of hydrazine and p-Nitrophenol

Scan rate variations were applied to investigate the electron transfer mechanism in gold electrode (GE) modified by samarium oxide (Sm_2O_3) nanoparticles for the detection of hydrazine and p-nitrophenol. Cyclic voltammograms with varying scan rates on hydrazine and p-nitrophenol are shown in Figs. 12a and b.

The voltammogram in Fig. 11. shows an increase in peak current response by varying the scan rate from 0.06 V/s to 0.48 V/s and 0.06 V/s to 0.96 V/s for 2 μM hydrazine and p-nitrophenol 2 μM since the reaction is controlled by mass transfer. This is related to the important role of the larger surface area of Sm_2O_3 nanoparticles, which contributes to increasing more efficient electron transfer in achieving catalytic performance for the analyte's hydrazine and p-nitrophenol. The increase in peak current and scan rate indicates the electrocatalytic reaction of hydrazine and p-nitrophenol on the modified GE surface. This variation is mainly caused by surface adsorption and diffusion processes on the surface layer of the modified electrode.

At lower scan rates, the diffusion process occurs relatively, and the analyte adsorption occurs at a slower rate during the mass transfer process. In contrast, at higher scan rates, the diffusion step becomes the

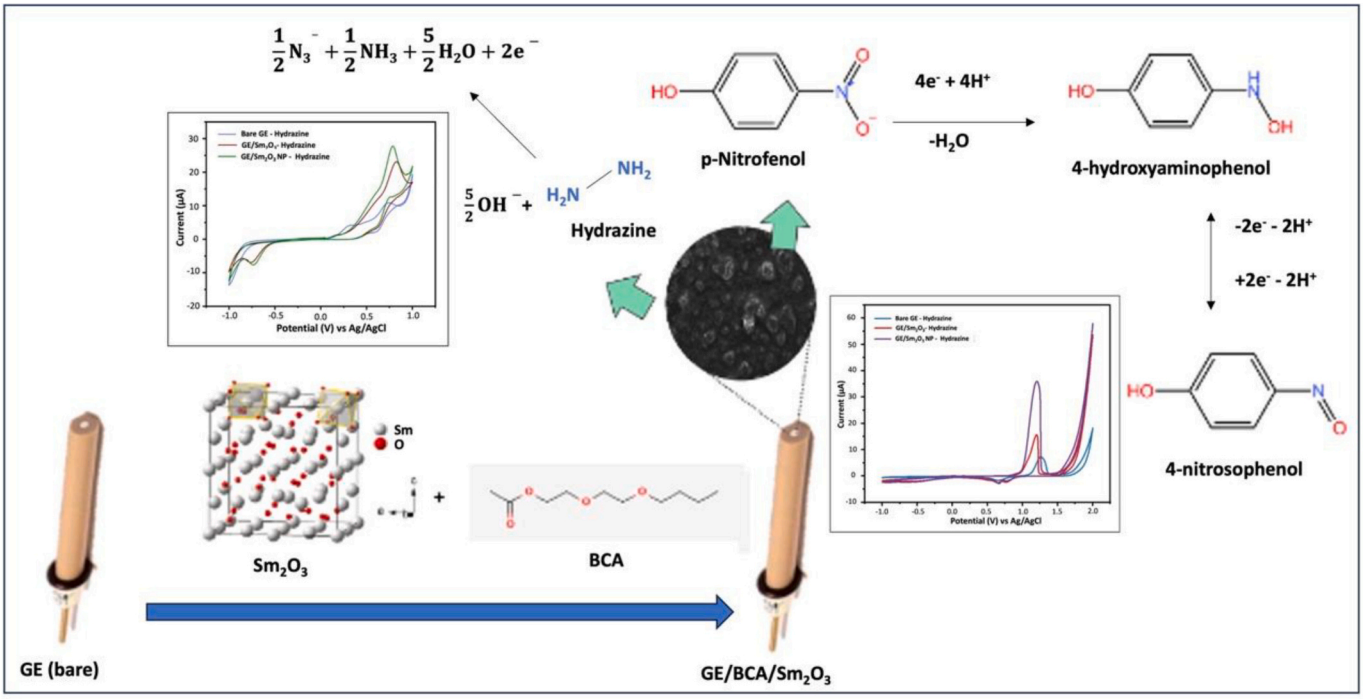

Fig. 11. Schematic illustration of hydrazine and p-nitrophenol detection via voltammetry using an electrode modified by Sm_2O_3 nanoparticles with the binding agent butyl carbitol acetate (BCA).

dominant factor in controlling the electrode reaction rate in the presence of external agents. In p-nitrophenol measurements, the reduction process and the redox couple exhibit a significant increase in the current response as a function of the scan rate.

The hydrazine measurements show that the oxidation is controlled mainly by the diffusion process on the GE surface modified with Sm_2O_3 nanoparticles. Based on the voltammogram of hydrazine measurements in Fig. 12a, the overpotential in the catalytic oxidation of hydrazine increases with the scan rate, indicating that there is a kinetic limitation in the reaction between the GE/Sm_2O_3 NP redox site and hydrazine. Therefore, the entire electrochemical reaction can be controlled by mass transfer and charge transfer kinetics.

3.5. Determination of analytical parameters

In this research, analytical parameters were determined by developing a calibration curve to determine the linearity, detection limit, recovery and repeatability of gold electrode (GE) modified samarium oxide (Sm_2O_3) GE/Sm_2O_3 nanoparticles in the detection of the two analytes, namely hydrazine, and p-nitrophenol. A calibration curve was created by varying the concentration of both analytes by 0, 0.1, 0.3, 0.5, 0.7, 0.9, 1.1, 1.3, 1.5, and 1.7 μM. The peak current response was measured using CV over a potential range of −1.0 V to 1.0 V and − 1.0 V to 2.0 V for hydrazine and p-nitrophenol with a scan rate of 0.06 V/s. Measurements were carried out three times for each concentration and the voltammogram results of the variation in concentrations are shown in Figs. 13a and b.

Based on the cyclic voltammogram illustrated in Fig. 13, the peak current response in the detection of hydrazine and p-nitrophenol with varying concentrations has shown a linear increase across a sufficiently wide concentration range. The resulting peak current increases with the concentration due to the oxidation or reduction of numerous hydrazine and p-nitrophenol analyte ions on the GE working electrode modified with Sm_2O_3 nanoparticles. This is consistent with the Rendless-Sevcik equation, indicating that the current is directly proportional to the analyte. The mechanism of electron transfer leads to a diffusion current where the magnitude is proportional to the analyte concentration. Subsequently, this concentration variation voltammogram is plotted against the current difference to develop a calibration curve (shown in Fig. 14 for hydrazine and Fig. 15 for p-nitrophenol).

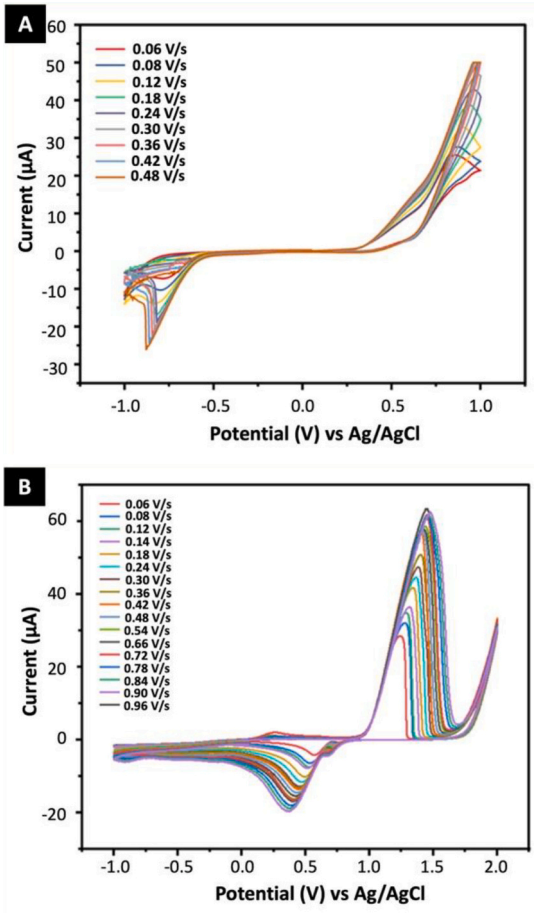

Fig. 12. Cyclic voltammogram of GE/Sm_2O_3 NPs for detection of (a) 2 μM hydrazine at scan rate variations of 0.06 V/s to 0.48 V/s and (b) 2 μM p-nitrophenol at 0.06 V scan rate variations/s to 0.96 V/s in 0.1 M PBS (pH 7.4).

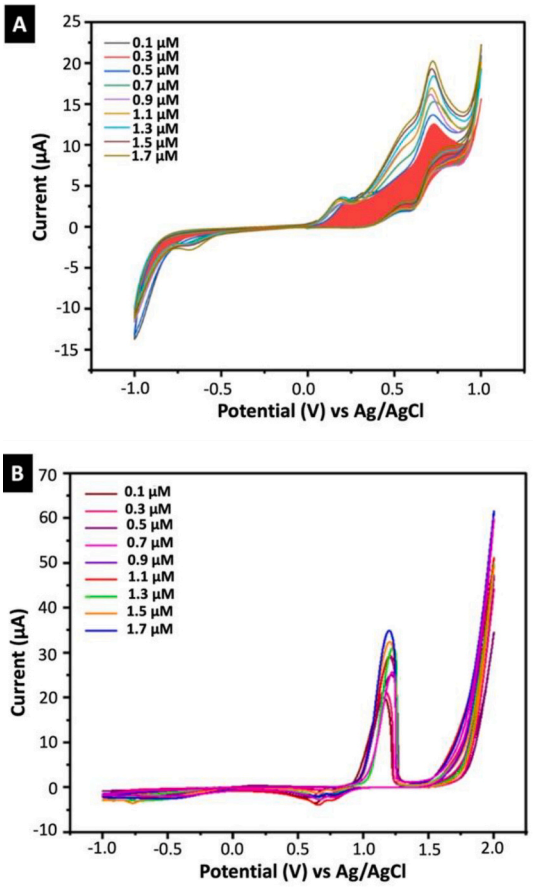

Fig. 13. Cyclic voltammogram of GE/Sm_2O_3 NP for detection at various concentrations (0.1; 0.3; 0.5; 0.7; 0.9; 1.1; 1.3; 1.5; and 1.7 μM) (a) hydrazine in the potential range of −1.0 V to 1.0 V and (b) p-nitrophenol in the potential range of −1.0 V to 2.0 V (in 0.1 M PBS (pH 7.4)).

The obtained calibration curve can be used for linear testing to determine the working area of the measurement and the sensitivity of GE modified with Sm_2O_3 nanoparticles.

This research obtains a calibration curve with a linear area in the concentration range of 0.1 μM to 1.7 μM. The calibration curve in Fig. 14 also shows the regression equation for hydrazine detection as $y = 5.6585\times + 10.57$ with correlation (R) and determination (R^2) coefficients of 0.9989 and 0.9980, respectively.

Furthermore, 10.57 represents the intercept (a), indicating the impact of the matrix, and a larger value shows a greater impact of the matrix on concentration measurements. Meanwhile, the 5.6585 represents the slope (b), reflecting the sensitivity of the method, namely the impact of changes in concentration on the resulting response, while a higher value shows greater sensitivity of the method. The line on the calibration curve represents a linear relationship in the data distribution between hydrazine concentration and current response. The generated

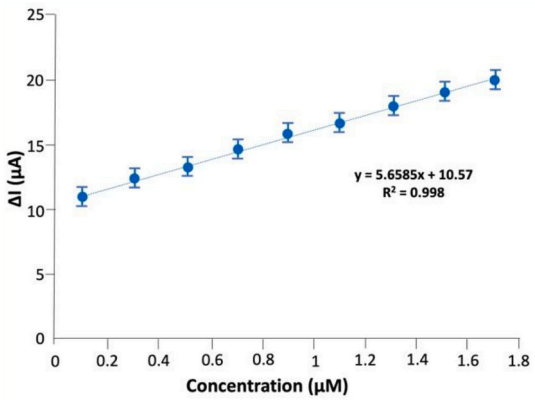

Fig. 14. The calibration curve of hydrazine detection with varying concentrations (0.1, 0.3, 0.5, 0.7, 0.9, 1.1, 1.3, 1.5, and 1.7 μM) within the potential range of −1.0 V to 1.0 V and a scan rate of 0.06 V/s in 0.1 M PBS (pH 7.4).

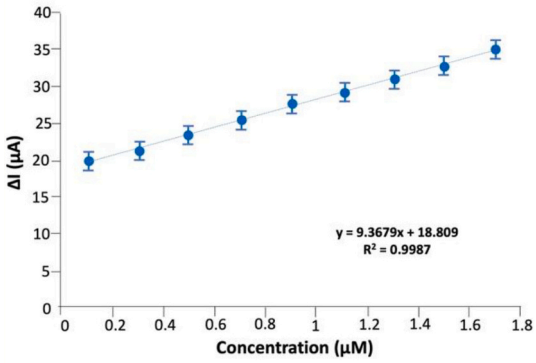

Fig. 15. The calibration curve of p-nitrophenol detection with varying concentrations (0.1, 0.3, 0.5, 0.7, 0.9, 1.1, 1.3, 1.5, and 1.7 μM) within the potential range of −1.0 V to 1.0 V and a scan rate of 0.06 V/s in 0.1 M PBS (pH 7.4).

regression model is valid and achieves an ideal linear relationship when the correlation coefficient (R) approaches 1 or $\geq$ 0.996. The correlation coefficient (R) in hydrazine detection is close to 1, specifically 0.9989, since the regression model is valid and has achieved an ideal linear relationship. Furthermore, the calibration curve can be used to calculate limit of detection (LoD) and limit of quantification (LoQ) by using the equation (LoD) = 3σ/slope and (LoQ) = 10σ/slope, where σ is the standard deviation for the particular system [20]. LoD and LoQ for hydrazine detection using GE/Sm_2O_3 NP are 0.4684 μM and 1.4194 μM, respectively. Based on the results, the values obtained are quite good, with a lower LoD for hydrazine measurement compared to [26] which used Gd_2O_3 in GE modification with LoD of 0.704 μM.

According to the regression equation, calculations can also be performed to determine recovery and repeatability. Recovery refers to the closeness of the current response from the analysis to the true values. This variable is determined by comparing the average measured concentrations with the true values. Meanwhile, repeatability is the closeness of the current response from one analysis to another during repeated measurements. The variable is measured as the variation coefficient, where a smaller standard deviation indicates a higher value. Recovery and repeatability of hydrazine detection are obtained through six measurements using a concentration of 0.1 μM at 98.74 % and 99.42 %. The obtained recovery and repeatability values show the closeness of the current response to variations in hydrazine concentration with the true values. In this context, the six times repetition of measurements is intended to minimize errors.

Based on Fig. 15, the calibration curve of p-nitrophenol detection is obtained with a linear area in the concentration range of 0.1 μM to 1.7 μM. The regression equation is y = 9.3679× + 18.809 with correlation (R) and determination (R^2) coefficients of 0.9993 and 0.9987. The generated regression model is valid and has achieved an ideal linear relationship with the correlation coefficient (R) approaching 1. The intercept (a) and slope (b) values obtained are 18.809 and 9.3679, indicating the sensitivity of the developed sensor. LoD and LoQ for p-nitrophenol detection using GE/Sm_2O_3 NP are 0.5033 μM and 1.5252 μM, respectively. Based on the results, the values obtained are fairly good, with a lower LoD for p-nitrophenol measurement compared to [26], which used Gd_2O_3 in GE modification with LoD of 1.527 μM. (See Table 1).

The determination of recovery and repeatability values for p-nitrophenol detection is obtained through six measurements using a p-nitrophenol concentration of 0.1 μM, resulting in 99.01 % and 98.45 %. The results obtained show the closeness of the current response to variations in p-nitrophenol concentration with the true values.

Moreover, repeatability and reproducibility of the Sm_2O_3 nanoparticles-modified GE electrochemical sensors were also tested in a real water sample for the further confirmation of the developed sensor. Based on Fig. 16, the obtained relative standard (RSD) figures of peak currents are found to be 3.3 % and 3.2 % for p-nitrophenol detection, which shows a good repeatability and reproducibility for the modified electrode.

4. Conclusion

In conclusion, GE/Sm_2O_3 NPs constitutes a promising candidate to be applied as an electrochemical sensor for the detection of hydrazine and p-nitrophenol due to its good recovery (98.74 and 99.01 %) and repeatability (99.42 and 98.45 %) for hydrazine and p-nitrophenol detection, respectively. These recovery rates suggest the sensor's excellent accuracy, meaning it can reliably measure hydrazine and p-nitrophenol concentrations in real-world samples. Its detection limit (LoD) was also found to be low at 0.4684 μM and 0.5033 μM at a concentration range of 0.1 to 1.7 μM for hydrazine and p-nitrophenol detection, respectively. Additionally, the GE's analytical parameter, such as reproducibility, was also tested in the real sample, which further shows a good result in terms of obtained RSD and recovery number. These results highlight the sensor's sensitivity and accuracy, making it suitable for detecting low concentrations of pollutants in environmental applications. The low LoD and LoQ are particularly important for early detection of contaminants, contributing to more effective pollution monitoring. This development provides valuable insight into the potential of Sm_2O_3-based sensors for improving environmental protection and monitoring practices.

Table 1
Research on electrochemical detection for hydrazine and p-nitrophenol.

Electrode	Analyte	Detection limit (μM)	Reference
Gold electrode/Gadolinium oxide nanoparticles	Hydrazine and p-nitrophenol	0.704 and 1.527	[26]
Gold electrode/Zink oxide	Hydrazine	2.2	[50]
Carbon Ceramic Electrode/Nickel hexacyanoferrate	Hydrazine	2.28	[51]
Glassy Carbon Electrode/Carbon Nanotubes	Hydrazine	2.0	[52]
Carbon Paste Electrode/Copper tetraphenylporphyrin onto zeolites cavity	Hydrazine and p-nitrophenol	1	[53]
Gold Electrode/Samarium oxide nanoparticles	Hydrazine and p-nitrophenol	0.4684 and 0.5033	This research

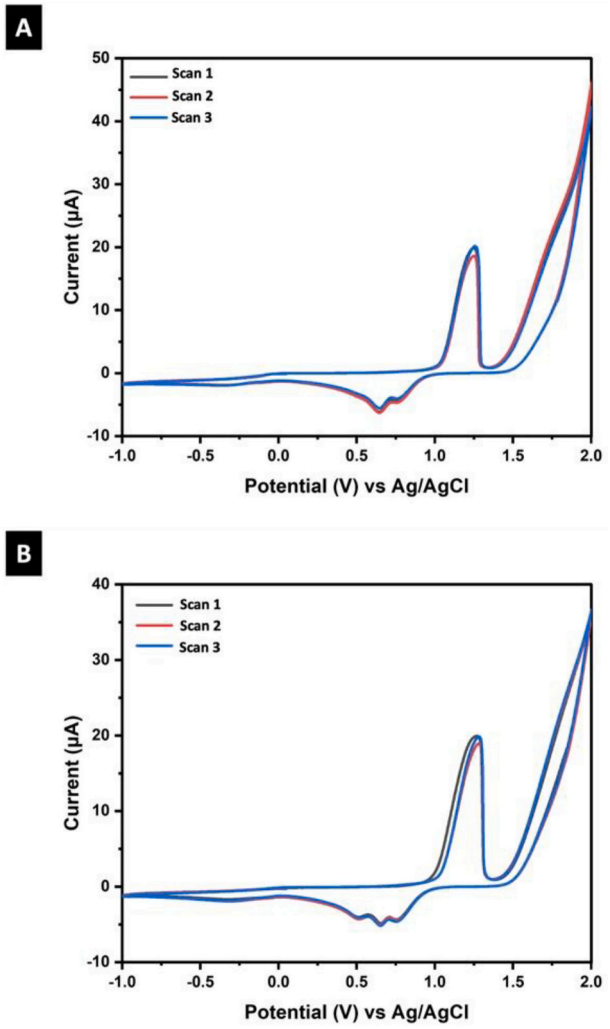

Fig. 16. Cyclic voltammogram of GE/Sm_2O_3 NP for p-nitrophenol detection at concentration of 1 μM in the potential range of −1.0 V to 2.0 V on Day 0 (A) and Day 7 (B) (in 0.1 M PBS (pH 7.4)).

CRediT authorship contribution statement

Santhy Wyantuti: Writing – original draft, Methodology, Funding acquisition, Formal analysis, Conceptualization. **Nur Azizah Ferdiana:** Methodology. **Sahlaa Alifah Zahra:** Formal analysis, Visualization, Writing – review & editing. **Retna Putri Fauzia:** Writing – review & editing, Writing – original draft, Visualization, Validation, Resources, Project administration, Methodology. **Irkham:** Visualization, Validation, Supervision. **Husain Akbar Sumeru:** Validation, Resources. **Qi Jia:** Writing – review & editing, Validation. **Dikdik Kurnia:** Supervision, Methodology, Investigation, Conceptualization. **Husein H. Bahti:** Supervision, Funding acquisition, Conceptualization.

Declaration of competing interest

The authors declare that they have no known competing financial interests or personal relationships that could have appeared to influence the work reported in this paper.

Acknowledgments

The authors are grateful for the financial support from the Padjadjaran Academic Recharging, Academic Leadership Grant (1458/UN6.3.1/PT.00/2024) and *Riset Kompetensi Dosen Unpad* (1959/UN6.3.1/PT.00/2024.) Universitas Padjadjaran, Indonesia for providing funding support.

Data availability

No data was used for the research described in the article.

References

[1] E. Popova-Kuznetsova, G. Tikhonowski, A.A. Popov, V. Duflot, S. Deyev, S. Klimentov, et al., Laser-ablative synthesis of isotope-enriched samarium oxide nanoparticles for nuclear nanomedicine, Nanomaterials 10 (2020) 1–11, https://doi.org/10.3390/nano10010069.

[2] T. Yousefi, M.T. Mostaedi, M. Ghasemi, A. Ghadirifar, A simple way to synthesize of samarium oxide nanoparticles: characterization and effect of pH on morphology, Synth. React. Inorg., Met.-Org., Nano-Met. Chem. 46 (2016) 137–142, https://doi.org/10.1080/15533174.2014.900795.

[3] M. Rahimi-Nasrabadi, S.M. Pourmortazavi, M. Aghazadeh, M.R. Ganjali, M. Sadeghpour Karimi, P. Novrouzi, Samarium carbonate and samarium oxide; synthesis, characterization and evaluation of the photo-catalytic behavior, J. Mater. Sci. Mater. Electron. 28 (2017) 5574–5583, https://doi.org/10.1007/s10854-016-6224-4.

[4] V. Adimule, P. Lakshminarayana, C. Bathula, B.H. Jeon, Insight into electro chemical and dielectric properties of flower shaped samarium embedded Y_2O_3@ SeO_2 nanocomposites for H_2O_2 sensor applications, Mater Today Commun. 38 (2024) 108163, https://doi.org/10.1016/j.mtcomm.2024.108163.

[5] B. Li, P. Wang, Development of a highly sensitive electrochemical sensor for dexamethasone detection using Fe_3O_4/polyaniline-cu(II) microspheres and hematite nanoparticles, Int. J. Electrochem. Sci. 19 (2024) 100622, https://doi.org/10.1016/j.ijoes.2024.100622.

[6] S.R. Jamnani, H.M. Moghaddam, S.G. Leonardi, G. Neri, A novel conductometric sensor based on hierarchical self-assembly nanoparticles Sm_2O_3 for VOCs monitoring, Ceram. Int. 44 (2018) 16953–16959, https://doi.org/10.1016/j.ceramint.2018.06.136.

[7] P.A. Pushpanjali, J.G. Manjunatha, B.M. Amrutha, N. Hareesha, Development of carbon nanotube-based polymer-modified electrochemical sensor for the voltammetric study of curcumin, Mater. Res. Innov. 25 (2021) 412–420, https://doi.org/10.1080/14328917.2020.1842589.

[8] N. Hareesha, J.G. Manjunatha, Z.A. Alothman, M. Sillanpää, Simple and affordable graphene nano-platelets and carbon nanocomposite surface decorated with cetrimonium bromide as a highly responsive electrochemical sensor for rutin detection, J. Electroanal. Chem. (2022) 917, https://doi.org/10.1016/j.jelechem.2022.116388.

[9] M.M. Charithra, J.G. Manjunatha, Electrochemical sensing of adrenaline using surface modified carbon nanotube paste electrode, Mater. Chem. Phys. (2021) 262, https://doi.org/10.1016/j.matchemphys.2021.124293.

[10] G. Tigari, J.G. Manjunatha, Poly(glutamine) film-coated carbon nanotube paste electrode for the determination of curcumin with vanillin: an electroanalytical approach, Monatsh. Chem. 151 (2020) 1681–1688, https://doi.org/10.1007/s00706-020-02700-8.

[11] M. Manjunatha Charithra, J.G. Manjunatha, Electrochemical sensing of paracetamol using Electropolymerised and sodium lauryl sulfate modified carbon nanotube paste electrode, ChemistrySelect 5 (2020) 9323–9329, https://doi.org/10.1002/slct.202002626.

[12] Chenthattil Raril, J.G. Manjunatha, D.K. Ravishankar, S. Fattepur, G. Siddaraju, L. Nanjundaswamy, Validated electrochemical method for simultaneous resolution of tyrosine, uric acid, and ascorbic acid at polymer modified Nano-composite paste electrode, Surf. Eng. Appl. Electrochem. 56 (2020) 415–426, https://doi.org/10.3103/S1068375520040134.

[13] T. Trinadh, H. Khuntia, T. Anusha, K.S. Bhavani, J.V.S. Kumar, P.K. Brahman, Synthesis and characterization of nanocomposite material based on graphene quantum dots and lanthanum doped zirconia nanoparticles: an electrochemical sensing application towards flutamide in urine samples, Diam. Relat. Mater. 110 (2020) 108143, https://doi.org/10.1016/j.diamond.2020.108143.

[14] J. Han, T. Wu, F. Li, M. Zhao, Y. Liu, M. Guo, et al., Highly sensitive methyl parathion electrochemical sensor designed from expired mung bean-derived porous carbon embellished with cerium oxide nanoparticles, Microchem. J. 201 (2024) 110678, https://doi.org/10.1016/j.microc.2024.110678.

[15] M.M. Khan, S.N. Matussin, Sm_2O_3 and Sm_2O_3-based nanostructures for photocatalysis, sensors, CO conversion, and biological applications, Cat. Sci. Technol. 13 (2023) 2274–2290, https://doi.org/10.1039/D2CY01976K.

[16] M. Arvand, S. Hemmati, Magnetic nanoparticles embedded with graphene quantum dots and multiwalled carbon nanotubes as a sensing platform for electrochemical detection of progesterone, Sensors Actuators B Chem. 238 (2017) 346–356, https://doi.org/10.1016/j.snb.2016.07.066.

[17] K. Alagumalai, R. Shanmugam, S.M. Chen, B. Thirumalraj, A.S. Haidyrah, C. Karuppiah, Impact of gadolinium oxide with functionalized carbon nanosphere: a portable advanced electrocatalyst for pesticide detection in aqueous environmental samples, Talanta 238 (2022) 123028, https://doi.org/10.1016/j.talanta.2021.123028.

[18] E.L.Y. Nasution, Analisis Karakterisasi Xrd Sintesis Gadolinium Karbonat $Gd_2(CO_3)_3$@PEG dengan Metode Solvotermal, J. Online Phys. 5 (2019) 29–32, https://doi.org/10.22437/jop.v5i1.8213.

[19] S. Wyantuti, B. Fadhilatunnisa, R.P. Fauzia, Q. Jia, A.A. Rahmani, et al., Response surface methodology box-behnken design to optimise the hydrothermal synthesis of gadolinium nanoparticles, Chin. J. Anal. Chem. 51 (2023) 100316, https://doi.org/10.1016/j.cjac.2023.100316.
[20] A. Ahab, F. Rohman, F. Iskandar, F. Haryanto, I. Arif, A simple straightforward thermal decomposition synthesis of PEG-covered Gd_2O_3 (Gd_2O_3@PEG) nanoparticles, Adv. Powder Technol. 27 (2016) 1800–1805, https://doi.org/10.1016/j.apt.2016.06.012.
[21] S. Kojima, L. Zhang, C. Kumar, H. Sumi, N. Ohta, H. Sekiguchi, et al., The effects of polyethylene glycol on the nucleation and growth of DNA-functionalized gold nanoparticles crystals, J. Cryst. Growth (2024) 127740, https://doi.org/10.1016/j.jcrysgro.2024.127740.
[22] C.C. Vidyasagar, Naik Y. Arthoba, Surfactant (PEG 400) effects on crystallinity of ZnO nanoparticles, Arab. J. Chem. 9 (2016) 507–510, https://doi.org/10.1016/j.arabjc.2012.08.002.
[23] Y. Rilda, F. Puspita, R. Refinel, A. Armaini, A. Agustien, H. Pardi, et al., Biosynthesis of ag-doped ZnO nanorods using template Bacillus sp. and polyethylene glycol via sol-gel-hydrothermal methods for antifungal application, S. Afr. J. Chem. Eng. 47 (2024) 91–97, https://doi.org/10.1016/j.sajce.2023.10.013.
[24] S.R. Jamnani, H.M. Moghaddam, S.G. Leonardi, G. Neri, PANI/Sm2O3 nanocomposite sensor for fast hydrogen detection at room temperature, Synth. Met. 268 (2020) 116493, https://doi.org/10.1016/j.synthmet.2020.116493.
[25] J. Anupriya, T. Senthilkumar, S.M. Chen, A precise electrochemical sensor based on Sm2O3/2D TiC hybrid for highly sensitive and selective detection of antihypertensive drug nimodipine, Colloids Surf. A Physicochem. Eng. Asp. 641 (2022) 128531, https://doi.org/10.1016/j.colsurfa.2022.128531.
[26] S. Chaudhary, S. Kumar, S. Kumar, G.R. Chaudhary, S.K. Mehta, A. Umar, Ethylene glycol functionalized gadolinium oxide nanoparticles as a potential electrochemical sensing platform for hydrazine and p-nitrophenol, Coatings 9 (2019) 1–15, https://doi.org/10.3390/coatings9100633.
[27] S.H. Guo, Z.Q. Guo, C.Y. Wang, Y. Shen, W.H. Zhu, An ultrasensitive fluorescent probe for hydrazine detection and its application in water samples and living cells, Tetrahedron 75 (2019) 2642–2646, https://doi.org/10.1016/j.tet.2019.03.022.
[28] G.E. Collins, S.L. Rose-Pehrsson, Sensitive, fluorescent detection of hydrazine via derivatization with 2,3-naphthalene dicarboxaldehyde, Anal. Chim. Acta 284 (1993) 207–215, https://doi.org/10.1016/0003-2670(93)80026-H.
[29] S.H. Guo, Z.Q. Guo, C.Y. Wang, Y. Shen, W.H. Zhu, An ultrasensitive fluorescent probe for hydrazine detection and its application in water samples and living cells, Tetrahedron 75 (2019) 2642–2646, https://doi.org/10.1016/j.tet.2019.03.022.
[30] R. Razavi, F. Garkani Nejad, S.A. Ahmadi, H. Beitollahi, Synthesis of ZnO@TiO_2 nanoparticles and its application to construct an electrochemical sensor for determination of hydrazine, Electrochem. Commun. 159 (2024) 107639, https://doi.org/10.1016/j.elecom.2023.107639.
[31] M.T. Vardini, N. Abbasi, A. Kaviani, M. Ahmadi, E. Karimi, Graphite electrode potentiometric sensor modified by surface imprinted silica gel to measure Valproic acid, Chem. Methodol. 6 (2022) 398–408, https://doi.org/10.22034/chemm.2022.328620.1437.
[32] A.B. Monnappa, J.G. Manjunatha, A.S. Bhatt, Design of a sensitive and selective voltammetric sensor based on a cationic surfactant-modified carbon paste electrode for the determination of alloxan, ACS Omega 5 (2020) 23481–23490, https://doi.org/10.1021/acsomega.0c03517.
[33] J.G. Manjunatha, C. Raril, N. Hareesha, M.M. Charithra, P.A. Pushpanjali, G. Tigari, et al., Electrochemical fabrication of poly (niacin) modified graphite paste electrode and its application for the detection of riboflavin, Open Chem. Eng. J. 14 (2021) 90–98, https://doi.org/10.2174/1874123102014010090.
[34] R.D. Crapnell, C.E. Banks, Electroanalytical overview: the electroanalytical sensing of hydrazine, Sensors Diagnostics 1 (2022) 71–86, https://doi.org/10.1039/d1sd00006c.
[35] S. Tajik, H. Beitollahi, F.G. Nejad, K. Zhang, Q. Van Le, H.W. Jang, et al., Recent advances in electrochemical sensors and biosensors for detecting bisphenol a, Sensors (Switzerland) 20 (2020) 1–18, https://doi.org/10.3390/s20123364.
[36] S. Tajik, M.B. Askari, S.A. Ahmadi, F.G. Nejad, Z. Dourandish, R. Razavi, et al., Electrochemical sensor based on $ZnFe_2O_4$/RGO nanocomposite for ultrasensitive detection of hydrazine in real samples, Nanomaterials (2022) 12, https://doi.org/10.3390/nano12030491.
[37] E. Saeb, K. Asadpour-Zeynali, Facile synthesis of TiO_2@PANI@Au nanocomposite as an electrochemical sensor for determination of hydrazine, Microchem. J. (2021) 160, https://doi.org/10.1016/j.microc.2020.105603.
[38] R. Razavi, F. Garkani Nejad, S.A. Ahmadi, H. Beitollahi, Synthesis of ZnO@TiO2 nanoparticles and its application to construct an electrochemical sensor for determination of hydrazine, Electrochem. Commun. 159 (2024) 107639, https://doi.org/10.1016/j.elecom.2023.107639.
[39] B. Kaur, R. Srivastava, B. Satpati, Copper nanoparticles decorated polyaniline-zeolite nanocomposite for the nanomolar simultaneous detection of hydrazine and phenylhydrazine, Cat. Sci. Technol. 6 (2016) 1134–1145, https://doi.org/10.1039/c5cy01064k.
[40] A. Othmani, Z. Kouki, S. Kouass, F. Touati, H. Dhaouadi, A highly sensitive hydrazine and hydrogen peroxide non-enzymatic sensor based on CuO nanoplatelets, J. Mater. Sci. Mater. Electron. 32 (2021) 3566–3576, https://doi.org/10.1007/s10854-020-05103-x.
[41] K. Ghanbari, Fabrication of silver nanoparticles-polypyrrole composite modified electrode for electrocatalytic oxidation of hydrazine, Synth. Met. 195 (2014) 234–240, https://doi.org/10.1016/j.synthmet.2014.06.014.
[42] H. Mohammad Shiri, A. Ehsani, Khales M. Jalali, Electrochemical synthesis of Sm2O3 nanoparticles: application in conductive polymer composite films for supercapacitors, J. Colloid Interface Sci. 505 (2017) 940–946, https://doi.org/10.1016/j.jcis.2017.06.086.
[43] M.M. Rahman, V.G. Alfonso, F. Fabregat-Santiago, J. Bisquert, A.M. Asiri, A. A. Alshehri, et al., Hydrazine sensors development based on a glassy carbon electrode modified with a nanostructured TiO_2 films by electrochemical approach, Microchim. Acta 184 (2017) 2123–2129, https://doi.org/10.1007/s00604-017-2228-x.
[44] R. Ahmad, N. Tripathy, D.-U.-J. Jung, Y.-B. Hahn, Highly sensitive hydrazine chemical sensor based on ZnO nanorods field-effect transistor, Chem. Commun. 50 (2014) 1890–1893, https://doi.org/10.1039/C3CC48197B.
[45] C.N.C. Hitam, A.A. Jalil, A review on exploration of Fe_2O_3 photocatalyst towards degradation of dyes and organic contaminants, J. Environ. Manag. 258 (2020) 110050, https://doi.org/10.1016/j.jenvman.2019.110050.
[46] A.R. Bhapkar, S. Bhame, A review on ZnO and its modifications for photocatalytic degradation of prominent textile effluents: synthesis, mechanisms, and future directions, J. Environ. Chem. Eng. 12 (2024) 112553, https://doi.org/10.1016/j.jece.2024.112553.
[47] J. Gao, Y. Zhao, W. Yang, J. Tian, F. Guan, Y. Ma, et al., Preparation of samarium oxide nanoparticles and its catalytic activity on the esterification, Mater. Chem. Phys. 77 (2003) 65–69, https://doi.org/10.1016/S0254-0584(01)00594-6.
[48] M.M. Khan, S.N. Matussin, Sm_2O_3 and Sm_2O_3-based nanostructures for photocatalysis, sensors, CO conversion, and biological applications, Cat. Sci. Technol. 13 (2023) 2274–2290, https://doi.org/10.1039/d2cy01976k.
[49] S. Alam, Q.Z. Khan, A. Gassoumi, M.I. Khan, M.Z. Iqbal, Z. Ahmad, Innovating synthesis approaches in advancing electrochemical efficiency: a journey into hydrothermal and sonochemical realms, J. Energy Storage 78 (2024) 109821, https://doi.org/10.1016/j.est.2023.109821.
[50] A. Umar, M.M. Rahman, Y.B. Hahn, ZnO nanorods based hydrazine sensors, J. Nanosci. Nanotechnol. 9 (2009) 4686–4691, https://doi.org/10.1166/jnn.2009.1103.
[51] A. Salimi, K. Abdi, Enhancement of the analytical properties and catalytic activity of a nickel hexacyanoferrate modified carbon ceramic electrode prepared by two-step sol–gel technique: application to amperometric detection of hydrazine and hydroxyl amine, Talanta 63 (2004) 475–483, https://doi.org/10.1016/j.talanta.2003.11.021.
[52] A. Salimi, L. Miranzadeh, R. Hallaj, Amperometric and voltammetric detection of hydrazine using glassy carbon electrodes modified with carbon nanotubes and catechol derivatives, Talanta 75 (2008) 147–156, https://doi.org/10.1016/j.talanta.2007.10.044.
[53] S.V. Guerra, L.T.K. Ubota, C.R.X. Avier, S.N. Akagaki, Experimental optimization of selective hydrazine detection in flow injection analysis using a carbon paste electrode modified with copper porphyrin occluded into zeolite cavity 15, 1999, pp. 1231–1234.
[54] S. Wyantuti, J. Iskandar, R. Putri Fauzia, H.H. Bahti, Optimization of hydrothermal synthesis of dysprosium oxide nanoparticles-attached-polyethyleneglycol template using response surface methodology-box-behnken, 2023.
[55] M.K. Barron, T.J. Young, K.P. Johnston, R.O.W. Iii, Investigation of processing parameters of spray freezing into liquid to prepare polyethylene glycol polymeric particles for, Drug Deliv. 4 (2003).
[56] A. López-Cudero, A. Cuesta, C. Gutiérrez, Potential dependence of the saturation CO coverage of Pt electrodes: the origin of the pre-peak in CO-stripping voltammograms. Part 1: Pt(111), J. Electroanal. Chem. 579 (2005) 1–12, https://doi.org/10.1016/j.jelechem.2005.01.018.
[57] K. Singh, A. Kaur, A. Umar, G.R. Chaudhary, S. Singh, S.K. Mehta, A comparison on the performance of zinc oxide and hematite nanoparticles for highly selective and sensitive detection of Para-nitrophenol, J. Appl. Electrochem. 45 (2015) 253–261, https://doi.org/10.1007/s10800-014-0762-3.